Current-Induced Magnetization Switching of Exchange-Biased NiO Heterostructures Characterized by Spin-Orbit Torque

Krzysztof Grochot,[1,2,*] Łukasz Karwacki,[3,†] Stanisław Łazarski,[1] Witold Skowroński,[1] Jarosław Kanak,[1] Wiesław Powroźnik,[1] Piotr Kuświk,[3] Mateusz Kowacz,[3] Feliks Stobiecki,[3] and Tomasz Stobiecki[1,2]

[1] *Department of Electronics, AGH University of Science and Technology, Al. Mickiewicza 30, 30-059 Kraków, Poland*

[2] *Faculty of Physics and Applied Computer Science, AGH University of Science and Technology, Al. Mickiewicza 30, 30-059 Kraków, Poland*

[3] *Institute of Molecular Physics, Polish Academy of Sciences, ul. Smoluchowskiego 17, 60-179 Poznań, Poland*

(Received 7 July 2020; revised 23 November 2020; accepted 8 December 2020; published 11 January 2021)

In this work, we study magnetization switching induced by spin-orbit torque in W (Pt)/Co/NiO heterostructures with variable thickness of W and Pt heavy-metal layers, a perpendicularly magnetized Co layer, and an antiferromagnetic NiO layer. Using current-driven switching and magnetoresistance and anomalous-Hall-effect measurements, we determine the perpendicular and in-plane exchange-bias field. Several Hall-bar devices possessing in-plane exchange bias from both systems are selected and analyzed in relation to our analytical switching model of the critical current density as a function of Pt and W thickness, resulting in estimation of the effective spin Hall angle and perpendicular effective magnetic anisotropy. We demonstrate in both the Pt/Co/NiO system and the W/Co/NiO system deterministic Co magnetization switching without an external magnetic field, which is replaced by an in-plane exchange-bias field. Moreover, we show that due to a higher effective spin Hall angle in the W-based system than in the Pt-based system, the relative difference between the resistance states in the magnetization current switching to the difference between the resistance states in magnetic field switching determined by the anomalous Hall effect ($\Delta R/\Delta R_{\mathrm{AHE}}$) is about twice as high in W-based devices than in Pt-based devices, while the critical switching-current density in W-based devices is 1 order lower than in Pt-based devices. The current-switching stability and the training process are discussed in detail.

DOI: 10.1103/PhysRevApplied.15.014017

I. INTRODUCTION

Spin-orbit-torque (SOT) random-access memories (RAMs) are anticipated as a next generation of low-power, high-endurance, nonvolatile, and energy-efficient magnetic RAMs, which fit into the modern trend of green information technology [1,2]. Spintronic data-storage devices, in contrast to their conventional semiconductor counterparts, need not be continuously refreshed, leading to the reduction of heat dissipation and lower energy consumption [3]. Recently, SOT-based technologies have evolved as one of the most promising, because they require neither high current densities nor high voltages applied to the thin tunnel barriers [4,5], and enable magnetization switching below 1 ns [6]. Such memory cells constitute an efficient alternative to spin-transfer-torque magnetoresistive RAM.

Significant progress has been achieved in understanding and utilizing the spin Hall effect [7–9] in heavy metals (HMs) or topological insulators [10] to control magnetic states of ferromagnets (FMs) and antiferromagnets (AFMs) [11]. The mechanism relies on SOT-induced switching due to accumulated spin density noncollinear with magnetization. However, the torque itself cannot switch the magnetization between two stable states without the up-down degeneracy along the charge-current flow direction being broken. It can be achieved by applying an external magnetic field collinear with the current (but noncollinear with the magnetization), which, however, is impractical in device applications and technologically unattractive. Several approaches have been proposed to replace the external magnetic field and achieve field-free switching: for example, magnetization switching controlled by the electric field in a hybrid ferromagnetic/ferroelectric structure [12], two coupled FM layers exhibiting magnetization easy axes orthogonal to each other [13–19], or introducing a lateral symmetry breaking

*grochot@agh.edu.pl
†karwacki@ifmpan.poznan.pl

by asymmetric layers [20–24]. However, one of the most-promising solutions is still the well-known exchange bias induced by interfacial exchange coupling a ferromagnet with an antiferromagnetic layer [25–28]. The use of a metallic antiferromagnet for this purpose has already been described in the literature [13,29], and it was shown to support both the spin Hall effect and exchange bias in a single layer. This setup, however, makes further optimization of SOT-induced switching of a ferromagnet difficult as the electron spin density generated in an AFM acts not only on the ferromagnet but also on the Néel order as well [30]. To distinguish between torques acting on ferromagnetic layers from the spin-orbit–induced effect and the exchange-bias effect, one can use a HM/FM coupled with an antiferromagnetic insulator such as NiO. It not only induces exchange bias [31–33] but also can enhance the perpendicular magnetic anisotropy (PMA) of the ferromagnetic layer [34] and allow one to achieve a lower critical switching current than in the case of metallic AFMs.

Use of HM/FM/NiO heterostructures as one of the elements in magnetoresistive RAMs is possible, as a recent study on NiO/MgO tunnel junctions has shown that there is a sizable tunneling magnetoresistance (TMR) [35], although its appearance is more complex than with use of a MgO barrier alone—the insertion of NiO leads to the appearance of a strong asymmetry in TMR and in particular to negative TMR [35]. It has also been shown that NiO alone can support large TMR in various magnetic tunnel junctions [36,37]. Moreover, there is a possibility for a novel type of memory cells, as it has been shown that NiO can mediate antidamping spin-transfer torque between metallic layers [38].

Motivated by the above-mentioned considerations, we present here a study of magnetization switching induced by spin-orbit torque in W (Pt)/Co/NiO heterostructures with variable thickness of the W and Pt layers, a perpendicularly magnetized Co layer, and an antiferromagnetic NiO layer. Using magnetoresistance measurements and current-driven magnetization switching, we demonstrate the simultaneous occurrence of in-plane ($H_{\mathrm{exb}}^{(x)}$) and perpendicular ($H_{\mathrm{exb}}^{(z)}$) components of the exchange-bias field. We show Co magnetization switching without an external magnetic field, which is replaced by an in-plane exchange-bias field, and for this case we develop an analytical magnetization-switching model of the critical current density. Finally, we discuss the current-switching stability and training process conducted on Hall-bar devices of Pt/Co/NiO and W/Co/NiO.

The remainder of this paper is organized as follows: Sec. II provides details of sample fabrication, and explains the experimental techniques used to characterize the samples, Sec. III describes the theoretical model for spin Hall threshold currents adopted for exchange-biased samples; Sec. IV contains the results and their discussion; and Sec. VI concludes and summarizes the paper.

II. EXPERIMENT

Two HM/FM/AFM multilayer systems consisting of two different heavy metals, W and Pt, are deposited. As shown schematically in Fig. 1(a) the bottom-up heterostructure is sequenced as $Si/SiO_2/W(Pt)/Co/NiO$. The heavy-metal layer is deposited in wedge-shaped form with thickness ranging from 0 to 10 nm along the 20-mm-long sample edge (x coordinate). The resulting thickness gradient is achieved by controlled movement of a shutter. The thicknesses of the two other layers, namely, Co and NiO, are 0.7 and 7 nm, respectively. We also deposit the Pt(4 nm)/Co(1 nm)/MgO system as a reference sample for further analysis. All metallic layers are deposited by magnetron sputtering at room temperature.

In the case of W sputtering, low dc power of 4 W and a 6-cm target-sample distance are used, which results in a deposition rate of 0.01 nm/s. Such conditions are essential for the growth of the W layer in the cubic β phase. Pt and Co are deposited with dc power of 8 and 15 W, respectively.

The stoichiometric NiO layer deposited on the top of Co layer is prepared from a NiO target by a pulsed-laser-deposition technique. The process is performed in a controlled oxygen atmosphere under O_2 partial pressure 1.5×10^{-5} mbar in a separate UHV chamber and samples are transferred between chambers without our breaking the UHV conditions. To induce exchange-bias coupling, a perpendicular magnetic field of 1.1 kOe is applied during deposition of the whole multilayer. Systematic studies of the perpendicular exchange-bias effect in the Au/Co/NiO/Au system by magneto-optical Kerr rotation, published in Ref. [34], have shown that the Co underlayer is oxidized due to deposition of NiO in an oxygen-rich atmosphere. Our x-ray-absorption-spectroscopy (XAS) studies at room temperature also confirm the surface oxidation of the Co layer to stoichiometric CoO [39,40] and prove that it is in a paramagnetic state (for details, see

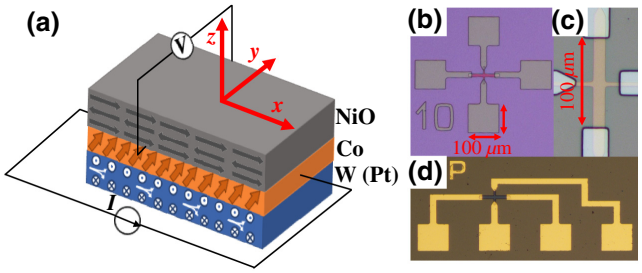

FIG. 1. (a) Our multilayer system. The orange arrows indicate the perpendicularly magnetized Co layer. The out-of-plane vectors on W (Pt)/Co interfaces show the accumulated spin as a result of the spin Hall effect. Optical microscopic images of the patterned Hall-bar device: (b) Hall-bar for magnetoresistance measurements, (c) detailed dimensions of the Hall bar, (d) Hall bar for SOT-induced magnetization-switching measurements.

Supplemental Material [41]). As shown in previous experimental work, exchange bias can not only be preserved but can also be enhanced by an insulating paramagnetic spacer [42,43]. On the other hand, XAS studies of the ordering of interfacial spins for antiferromagnetic bilayer Co/NiO show that an adjacent NiO layer can increase the CoO layer's Néel temperature (T_N) due to the strong exchange interaction at the CoO/NiO interface [44,45]. For this reason, it cannot be definitely ruled out that the exchange bias on the Co layer may come from the antiferromagnetic CoO/NiO bilayer. Moreover, in both cases, the oxidation process effectively reduces the ferromagnetic thickness of Co, which leads to an increase in the surface anisotropy, revealing strong PMA of Co. Nevertheless, this issue requires further investigations, which is beyond the scope of this paper.

The thicknesses of all layers are determined from the deposition growth rate of particular materials calibrated by x-ray-reflectivity measurements. Next, all as-deposited samples are characterized before patterning by x-ray diffraction ($\theta - 2\theta$) and grazing-incidence x-ray diffraction (for details, see Supplemental Material [41]). All systems are also examined with a polar Kerr magnetometer to determine the range of HM thicknesses for which PMA occurs. Square hysteresis loops are observed, which indicate the presence of PMA in both systems for Pt-layer thickness t_{Pt} between 1 and 9 nm and for W-layer thickness t_{W} between 3.5 and 8 nm, which is confirmed by anomalous-Hall-effect (AHE) measurements (see Supplemental Material [41]).

After basic characterization of continuous samples, both heterostructures are patterned by optical direct-imaging lithography and ion etching to create a matrix of Hall-bar devices with different t_{HM} for subsequent electrical measurements [Figs. 1(b)–1(d)]. The sizes of the prepared structures are $100 \times 10\ \mu\mathrm{m}^2$ for magnetoresistance and AHE measurements and $30 \times 30\ \mu\mathrm{m}^2$ for current-induced-magnetization-switching experiments. Al(20 nm)/Au(30 nm) electrical leads of $100 \times 100\ \mu\mathrm{m}^2$ are deposited in a second lithography step followed by the lift-off process. Specific locations of pads near the Hall-bars are designed for measurement in a custom-made rotating probe station allowing two-point or four-point measurement of electrical transport properties in the presence of the magnetic field applied at arbitrary azimuthal and polar angles with respect to the Hall-bar axis.

The resistance of each Hall bar is measured by a four-point method [46] and the resistivities of the Pt and W layers are determined with a parallel-resistor model and the method described by Kawaguchi *et al.* [47]. Analysis of the Pt and W resistivities yielded 30 $\mu\Omega\,\mathrm{cm}$ [14,47–49] and 170 $\mu\Omega\,\mathrm{cm}$ [49–52], respectively. The Co resistivity is 28 $\mu\Omega\,\mathrm{cm}$ when Co is deposited on Pt [14] and 58 $\mu\Omega\,\mathrm{cm}$ when Co is deposited on W. The details of the resistivity measurements are presented in Supplemental Material [41].

III. CRITICAL-CURRENT MODEL

To determine the influence of exchange bias on the threshold current in our system, we follow the analysis for spin Hall threshold currents first derived by Lee *et al.* [53,54].

We start with the Landau-Lifshitz-Gilbert equation for macrospin magnetization: $\hat{\mathbf{m}} = (m_x, m_y, m_z) = (\cos\phi \sin\theta, \sin\phi \sin\theta, \cos\theta)$,

$$\frac{d\hat{\mathbf{m}}}{dt} - \alpha\hat{\mathbf{m}} \times \frac{d\hat{\mathbf{m}}}{dt} = \mathbf{\Gamma}, \tag{1}$$

where α is the Gilbert damping constant.

The general torque exerted on magnetization assumes the following form:

$$\mathbf{\Gamma} = -\gamma_0\hat{\mathbf{m}} \times \mathbf{H}_{\mathrm{eff}} - \gamma_0 H_{\mathrm{DL}}\hat{\mathbf{m}} \times \hat{\mathbf{m}} \times \hat{\mathbf{y}}, \tag{2}$$

where γ_0 is the gyromagnetic constant, and the first term comes from the effective field, $\boldsymbol{H}_{\mathrm{eff}} = -\nabla_{\boldsymbol{m}} u$, where free energy of the FM has the form

$$u = -\frac{1}{2}H_{K,\mathrm{eff}}m_z^2 - \frac{1}{2}H_A m_y^2 - m_x H_x - m_x H_{\mathrm{exb}}^{(x)}, \tag{3}$$

where $H_{K,\mathrm{eff}}$ is the field of the effective perpendicular magnetic anisotropy, H_A is field of the effective in-plane anisotropy, H_x is the magnetic field along the x direction, and $H_{\mathrm{exb}}^{(x)}$ is the in-plane exchange bias.

The second torque term in Eq. (2) comes from the dampinglike field,

$$H_{\mathrm{DL}} = \frac{\hbar}{2e\mu_0 M_s t_{\mathrm{FM}}}\theta_{\mathrm{SH}} j_{\mathrm{HM}} \left(1 - \operatorname{sech}\frac{t_{\mathrm{HM}}}{\lambda_{\mathrm{HM}}}\right)\frac{g_r}{1+g_r}, \tag{4}$$

where $\hbar$ is the reduced Planck's constant, e is the elementary charge, $\mu_0 M_s$ is saturation magnetization, t_{FM} is the thickness of ferromagnetic layer, θ_{SH} is the spin Hall angle, j_{HM} is the current density flowing through HM, and $g_r = 2\lambda_{\mathrm{HM}}\rho_{\mathrm{HM}}G_r \coth(t_{\mathrm{HM}}/\lambda_{\mathrm{HM}})$ is the unitless real part of the spin-mixing conductivity, G_r, where λ_{HM}, ρ_{HM}, and t_{HM} are the HM's spin diffusion length, resistivity, and thickness, respectively. The dampinglike field is induced by $\hat{\mathbf{y}}$-polarized spin accumulation due to the spin Hall effect in the HM.

The stationary solution of the Landau-Lifshitz-Gilbert equation (1) leads to the torque equilibrium condition, $\mathbf{\Gamma} = 0$. For a strong magnetic field applied along the x direction, we assume $\phi \approx 0$, which leads to the following condition

for the dampinglike field:

$$H_{\mathrm{DL}} = \cos\theta \left(H_{\mathrm{exb}}^{(x)} - H_{K,\mathrm{eff}} \sin\theta + H_x \right). \tag{5}$$

By analyzing the stability of the above equation, we obtain a simplified relation for the critical dampinglike field:

$$H_{\mathrm{DL}}^{\mathrm{sw}} \approx \frac{H_{K,\mathrm{eff}}}{2} - \frac{H_x - H_{\mathrm{exb}}^{(x)}}{\sqrt{2}}. \tag{6}$$

Inserting into the above equation the explicit formula for the dampinglike field, Eq. (4), we obtain the following expression for the critical current density:

$$j_c^{\mathrm{sw}} \approx \frac{2e\mu_0 M_s t_{\mathrm{FM}} (1 + g_r)}{\hbar\theta_{\mathrm{SH}} g_r \left(1 - \operatorname{sech} \frac{t_{\mathrm{HM}}}{\lambda_{\mathrm{HM}}}\right)} \left(\frac{H_{K,\mathrm{eff}}}{2} - \frac{H_x - H_{\mathrm{exb}}^{(x)}}{\sqrt{2}} \right). \tag{7}$$

Assuming a perfect HM/FM interface (i.e., $G_r \to \infty$) and assuming $t_{\mathrm{HM}} \gg \lambda_{\mathrm{HM}}$ leads to the simplified expression

$$j_c^{\mathrm{sw}} \approx \frac{2e\mu_0 M_s t_{\mathrm{FM}}}{\hbar\theta_{\mathrm{SH}}} \left(\frac{H_{K,\mathrm{eff}}}{2} - \frac{H_x - H_{\mathrm{exb}}^{(x)}}{\sqrt{2}} \right), \tag{8}$$

which is used later to fit the experimental data. Our model does not take into account the switching mechanism due to creation and motion of domain walls, which has been observed in the Pt/Co system [55] and results in a smaller switching-current density than that estimated by the model above. Our estimate can, however, be treated as the upper limit.

IV. RESULTS AND DISCUSSION

A. SOT-induced current switching

The anomalous Hall effect is used to determine the current-driven magnetization switching between high-stable-resistance and low-stable-resistance states. The measurement setup is shown in Fig. 1(a). Initially, the sample is magnetized by an external magnetic field applied along the z direction to the state corresponding to low resistance of the AHE loop.

Then, a sequence of current pulses with 10-ms duration and 20-ms intervals in the x direction is applied to drive the magnetization switching. The current is swept from negative to positive and back to negative and simultaneously the transverse voltage is measured in the presence of an in-plane magnetic field, collinear with the current direction (H_x). The value of H_x is changed sequentially after each switching loop.

As a result, we obtain the current-switching loops for Pt-based and W-based Hall-bar devices [Figs. 2(a) and 2(b)].

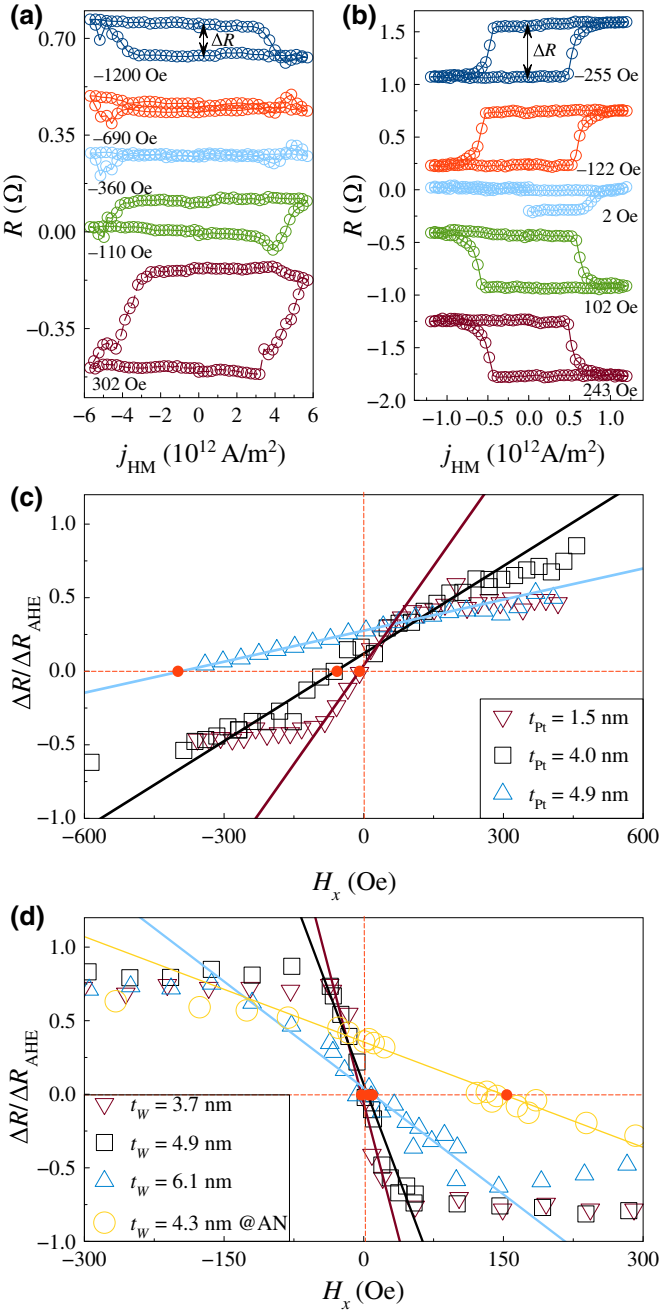

FIG. 2. Examples of the current-switching loops for different values of the external magnetic field H_x in the Pt(4.9 nm)/Co/NiO system (a) and the W(4.9 nm)/Co/NiO system (b). The ratio $\Delta R/R_{\mathrm{AHE}}$ is depicted in (c),(d); the intersection is marked by a red dot. $H_{\mathrm{exb}}^{(x)}$ in the Pt-based system is 5 Oe for $t_{\mathrm{Pt}} = 1.5$ nm, 60 Oe for $t_{\mathrm{Pt}} = 4.0$ nm, and 392 Oe for $t_{\mathrm{Pt}} = 4.9$ nm. For all analyzed W elements, the values are approximately 0 Oe in the measurement error limit and −148 Oe for the annealed sample (@AN).

Opposite loop polarities result in Pt having a positive spin Hall angle and W having a negative one.

By analyzing the difference between high and low AHE resistance from the AHE loop for different thicknesses

of Pt-based and W-based devices, we determine ΔR_{AHE}. Next, the current-switching loop opening ΔR is measured, for each value of the applied magnetic field H_x, which shows a closing loop with decreasing H_x [Figs. 2(a) and 2(b)]. The $\Delta R/\Delta R_{\mathrm{AHE}}$ ratio as a function of H_x, which is a measure of the effectiveness of current-induced magnetization switching for Pt-based and W-based devices, is shown in Figs. 2(c) and 2(d). The dependence obtained is approximately linear for small positive and negative H_x. As can be seen, ΔR does not reach ΔR_{AHE}, even when a large magnetic field is applied (see also Fig. S10 in Supplemental Material [41]).

The intersection of the linear function with zero $\Delta R/\Delta R_{\mathrm{AHE}}$, corresponding to the magnetic field for which the loop is closed, can be identified as the value of H_x that compensates the in-plane component of the exchange-bias field ($H_{\mathrm{exb}}^{(x)}$) and allows us to indirectly determine the value of $H_{\mathrm{exb}}^{(x)}$, because the aforementioned in-plane compensation field has the same value, but the opposite sign.

The intersection points for the Pt-based system depend on the Pt-layer thickness, reaching maximal compensation-field magnitude for $t_{\mathrm{Pt}} = 4.9$ nm, while in the W-based structure, intersection occurs roughly at zero H_x field in a wide range of W-layer thicknesses, as shown in Fig. 3. In high H_x fields, ΔR saturates, for W-based devices reaching about $0.8\Delta R_{\mathrm{AHE}}$ [Fig. 2(d)], while for Pt-based devices it changes with increasing Pt thickness from about $0.5\Delta R_{\mathrm{AHE}}$ to $0.28\Delta R_{\mathrm{AHE}}$ [Fig. 2(c) and Fig. S10(a) in Supplemental Material [41]]. The perpendicular exchange-bias field ($H_{\mathrm{exb}}^{(z)}$), determined by AHE hysteresis, is highest for a HM thickness of about 5 nm in both systems, but $H_{\mathrm{exb}}^{(z)}$ in the W-based system is 2 times smaller than in the Pt-based system (see Fig. S7 in Supplemental Material [41]).

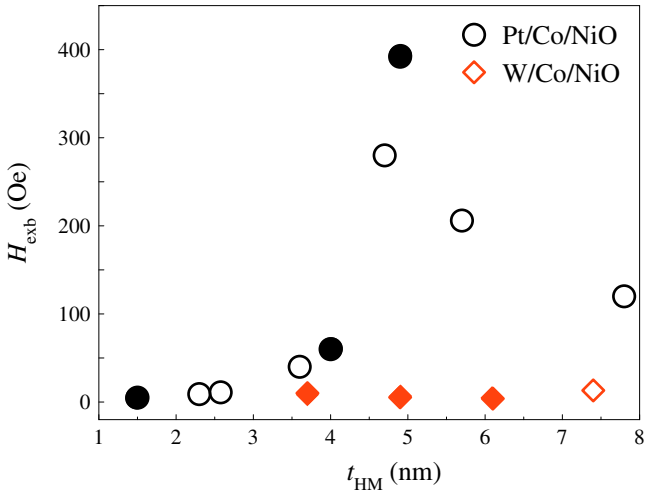

FIG. 3. $H_{\mathrm{exb}}^{(x)}$ obtained from ΔR zero shifts for the as-deposited W(Pt)/Co/NiO system. Filled points mark the elements for which the theoretical threshold-current model is fitted.

Because in the as-deposited W/Co/NiO heterostructure the magnitude of $H_{\mathrm{exb}}^{(x)}$ is negligible, field-free SOT-induced magnetization switching is not achieved. Therefore, to induce the in-plane component of exchange bias, the system is annealed at 100 °C (i.e., at a temperature slightly higher than the blocking temperature of 373 K but lower than T_N of 525 K) for 15 min and then cooled to room temperature in the presence of an external magnetic field of 4 kOe applied perpendicularly to the sample. Afterward, the remeasured AHE loop for the selected HM thickness indicates the presence of the PMA and $H_{\mathrm{exb}}^{(z)}$ in the Co layer, manifested by a rectangular-shape shift of −67 Oe [see Fig. S6(b) in Supplemental Material [41]]. In the next step, the current-switching experiments are repeated and results are analyzed as described above. Finally, $H_{\mathrm{exb}}^{(x)} = -148$ Oe is obtained from ΔR measurements [see Fig. S10(b) in Supplemental Material [41]]. For further analysis and fitting our threshold-current model in an exchange-biased system, three as-deposited Pt/Co/NiO Hall-bar devices with Pt thicknesses of 1.5, 4.0, and 4.9 nm are selected and denoted as A2, A3, and A4, respectively. We select also three as-deposited W/Co/NiO Hall-bar devices of with W thicknesses of 3.7, 4.9, and 6.1 nm which are denoted as B1, B2, and B3, respectively, and chose the annealed W(4.3 nm)/Co/NiO device (C1). We also fit our model to the reference sample (denoted A1), which is used to verify the model, as indicated earlier.

B. In-plane exchange bias

To confirm the above-discussed $H_{\mathrm{exb}}^{(x)}$, the resistance along the Hall bar (R_{xx}) is measured with the external magnetic field being swept along the x direction and is modeled with the equation

$$R_{xx} = R_0 + \Delta R_{\mathrm{AMR}} m_x^2, \tag{9}$$

where R_0 is the magnetization-independent resistance and ΔR_{AMR} denotes changes due to the anisotropic magnetoresistance effect. Considering the equilibrium condition of energy density [Eq. (3)] with respect to angle ϕ, the longitudinal resistance is reformulated to

$$R_{xx} \approx R_0 + \Delta R_{\mathrm{AMR}} \frac{(H_{\mathrm{exb}}^{(x)} + H_x)^2}{H_A^2}. \tag{10}$$

Measured R_{xx} for samples A2–A4, B1–B3, and C1 is shown in Fig. 4. A parabolic function is fitted to the data points, and minima of the functions are indicated with arrows. According to Eq. (10), the minima can be identified as the $H_{\mathrm{exb}}^{(x)}$ field, as discussed in the previous section. The resulting values for samples A2, A3 and A4 of about 6, 176, and 522 Oe [Figs. 4(d)–4(f)], respectively, are consistent with the ones obtained in the ΔR opening loop of the current-switching experiment described in Sec. IV A.

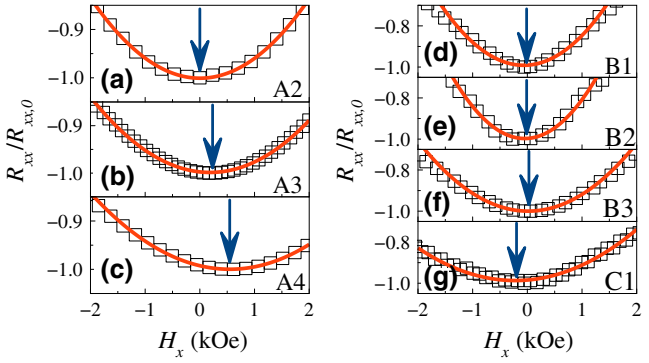

FIG. 4. $H_{\mathrm{exb}}^{(x)}$ obtained from $R_{xx}(H_x)$ measurements for as-deposited Pt-based systems (a)–(c) and W-based systems (d)–(f) and the annealed W/Co/NiO system (g). The blue arrows indicate the position of in-plane $H_{\mathrm{exb}}^{(x)}$. Experimental data are normalized to a minimum point. The red lines are fits according to Eq. (10).

As-deposited B-series Hall bars still exhibit negligible loop shifts [Figs. 4(d)–4(f)]. The only exception is the annealed C1 element, for which the value is −158 Oe [Fig. 4(g)]. $H_{\mathrm{exb}}^{(x)}$ values obtained from magnetoresistance measurements are in general less noisy and are used for further analysis.

C. Fitting procedure

For the analysis of the SOT-induced magnetization switching, we use AHE resistance hysteresis loops versus applied current densities in the HM layer (j_{HM}) measured in a different external magnetic field H_x; examples are depicted in Fig. 5.

First, using a derivative of $(\partial V_{\mathrm{AHE}}/\partial j_{\mathrm{HM}})$, we calculate the threshold switching current (j_c^{sw}) separately for each H_x. As a result, linear dependencies of j_c^{sw} versus H_x are obtained for selected Pt and W thicknesses. Nevertheless, a large number of free parameters in the model equation [Eq. (8)] may cause large uncertainties in the determined values. For this reason, the first part of Eq. (8) is replaced by a single parameter a, which is fixed and calculated as the linear slope coefficient determined by numerical differentiation of the j_c^{sw} dependence. Therefore, Eq. (8) can be rewritten as

$$j_c^{\mathrm{sw}} \approx a\left(\frac{H_{K,\mathrm{eff}}}{2} - \frac{H_x - H_{\mathrm{exb}}^{(x)}}{\sqrt{2}}\right), \tag{11}$$

where a is a fixed parameter obtained from differing j_c^{sw}-dependence data points.

This ensures that the only free-fit parameter is $H_{K,\mathrm{eff}}$. As mentioned earlier, $H_{\mathrm{exb}}^{(x)}$ is a fixed parameter obtained from the magnetoresistance measurements.

Initially, the model is verified on the reference sample A1, which is characterized by zero $H_{\mathrm{exb}}^{(x)}$. In this particular case, both $H_{\mathrm{exb}}^{(x)}$ and $H_{K,\mathrm{eff}}$ are set as free parameters to check the validity of the parameters obtained from fitting. As expected, $H_{\mathrm{exb}}^{(x)} = 0$ Oe and $H_{K,\mathrm{eff}} = 2508$ Oe are obtained with a very good compliance level of $R^2 = 0.93$.

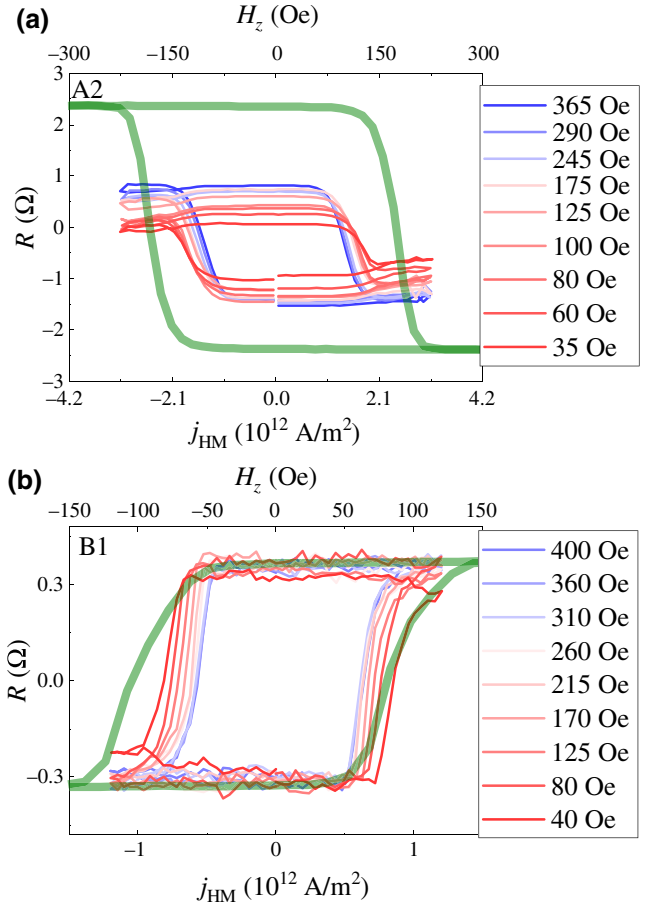

FIG. 5. Examples of a series of current-switching hysteresis loops for sequentially changed values of H_x in two selected elements, A2 (a) and B1 (b). Anomalous Hall resistances are represented by the green line.

Next, a simplified model equation [Eq. (11)] is fitted to all selected Pt/Co/NiO and W/Co/NiO samples. As indicated, $H_{\mathrm{exb}}^{(x)}$ is fixed and set in accordance with Table I. The fitting results are depicted in Fig. 6, where the solid lines correspond to the model equation for all devices investigated. As shown, the model exhibits good correlation with the data points. All of the R^2 coefficients are above 0.90, ensuring a low uncertainty level. For higher H_x, there are deviations from a linear dependence in both systems.

In case of W-based devices, the deviations appear at lower H_x field than in Pt-based devices. This can be explained by the lower $H_{K,\mathrm{eff}}$ (see Table I) for as-deposited W/Co/NiO systems than for as-deposited Pt/Co/NiO systems. Devices of the A series are characterized by increased $H_{K,\mathrm{eff}}$ and H_c with increasing Pt thickness [Figs. 6(b)–6(d)]. Additionally, annealing of the B-series

TABLE I. In-plane exchange-bias field ($H_{\text{exb}}^{(x)}$), effective anisotropy field ($H_{K,\text{eff}}$), spin Hall angle ($\theta_{\text{SH,eff}}$), and saturation magnetization ($\mu_0 M_s$) obtained as a result of magnetoresistance measurements and fitting the threshold-current model to the experimental data.

			Pt/Co/MgO		
Sample	t_{Pt} (nm)	$H_{\text{exb}}^{(x)}$ (Oe)	$H_{K,\text{eff}}$—fit (Oe)	$\theta_{\text{SH,eff}}$—fit (%)	$\mu_0 M_s$ (T)
A1	4.0	0	2508± 80	13.5 ± 1	0.5
			Pt/Co/NiO		
Sample	t_{Pt} (nm)	$H_{\text{exb}}^{(x)}$ (Oe)	$H_{K,\text{eff}}$—fit (Oe)	$\theta_{\text{SH,eff}}$—fit (%)	$\mu_0 M_s$ (T)
A2	1.5	6 ± 1	2141 ± 10	4.1 ± 0.8	0.5
A3	4.0	176 ± 3	4130 ± 10	5.2 ± 1.2	0.5
A4	4.9	522 ± 14	4638 ± 10	5.8 ± 1.3	0.5
			W/Co/NiO		
Sample	t_{W} (nm)	$H_{\text{exb}}^{(x)}$ (Oe)	$H_{K,\text{eff}}$—fit (Oe)	$\theta_{\text{SH,eff}}$—fit (%)	$\mu_0 M_s$ (T)
B1	3.7	0	1132 ± 20	−5.7 ± 1.1	0.5
B2	4.9	30 ± 15	1031 ± 10	−7.5 ± 1.5	0.5
B3	6.1	7 ± 1	1035 ± 11	−9.3 ± 1.8	0.5
C1	4.3	−158 ± 29	2584 ± 2	−44.0 ± 5	0.5

devices results in doubling of the $H_{K,\text{eff}}$ value with increasing H_c.

Finally, we calculate the effective spin Hall angles ($\theta_{\text{SH,eff}}$) in the HM layer. For the calculations we use magnetization saturation ($\mu_0 M_s$) of 0.5 T in both systems, obtained from VSM measurements (see Fig. S11 in Supplemental Material [41]). We also assume an infinite value of mixing conduction (g_r), which is mostly valid for metallic interfaces [56].

The assumptions we make allow us to calculate the effective spin Hall angle from the following formula:

$$\theta_{\text{SH,eff}} = \frac{2e\mu_0 M_s t_F}{\hbar a}. \tag{12}$$

The values of $\theta_{\text{SH,eff}}$ obtained are listed in Table I and agree with the ones found in the literature [14,48,49,51,57–65]. $\theta_{\text{SH,eff}}$ values in as-deposited B-series devices are slightly higher than the values calculated for A-series devices, which combined with significantly lower $H_{K,\text{eff}}$ results in critical switching-current densities that are approximately approximately 1 order of magnitude smaller in this system. It is also worth noting that annealing of the W-based system, apart from inducing $H_{\text{exb}}^{(x)}$, also increases $\theta_{\text{SH,eff}}$ to −44% [51,62–64] and reduces j_c^{sw} by 1 order of magnitude [Fig. 6(h)]. To confirm the high value of $\theta_{\text{SH,eff}}$, a current-switching experiment is performed on another annealed sample from the same series. A similar $\theta_{\text{SH,eff}}$ value is obtained (see Fig. S9 in Supplemental Material [41]). We attribute a high value of the effective spin Hall angle of W similarly as in Refs. [49,51,63,64] to the highly resistive β-W phase. For example $\theta_{\text{SH,eff}}$ is approximately −30% at room temperature and more than −50% at 50 K in Ref. [62], while in Ref. [64] it is approximately −44%. Recently, McHugh *et al.* [65] showed, from first-principles calculations, that interstitial O and N dopants help to stabilize β-W grains during film deposition, and this process leads to high spin Hall angles.

D. Training effect

The training effect in both systems is also investigated for verification of the thermal stability of the heterostructures examined. To do this, pulses 10 times longer than those used in the experiments described in Sec. IV A are used. For this purpose, multiple current switching in a fixed external H_x field is performed by 100-ms current pulses with a 200-ms interval between them. The magnitude of the external H_x field is chosen to obtain magnetization switching. The series of current-switching loops depicted in Figs. 7(a) and 7(b) are obtained. Next, loop opening ΔR and critical current densities j_c^{sw} are determined as a function of loop numbers. The results are presented in Figs. 7(c) and 7(d).In both systems, j_c^{sw} and ΔR decrease with increasing number of magnetization switches, and their dependence on the number of loops is similar. During the first few switching events, a significant reduction in both ΔR and j_c^{sw} is observed. These phenomena can be explained by the progressively increasing temperature in both systems due to Joule heating [29] and the training effect [28,66,67], witnessed also during magnetic field switching [28,68,69]. It is worth mentioning that the Joule-heating effect leads to a reduction of the switching current and anisotropy. Saturation of the dependence is caused by achieving a balance between the generated heat and the emitted heat. This saturation occurs for smaller repetition number in the system with Pt (after about 20 switches) in contrast to the Pt-based system, in which it is not reached even after 35 switches.

Furthermore, for the Pt-based system we investigate how the number of switches affects $H_{\text{exb}}^{(x)}$. For this purpose, we measure the longitudinal magnetoresistance signal, R_{xx}, as in Sec. IV B, before the current-switching experiment, and we find that $H_{\text{exb}}^{(x)}$ is 302 Oe [Fig. 8(a)]. First, the current is switched several times in zero external magnetic field. It is found that $H_{\text{exb}}^{(x)}$ decreases to 0 Oe [Fig. 8(b)]. This proves that thermal energy generated during the pulses

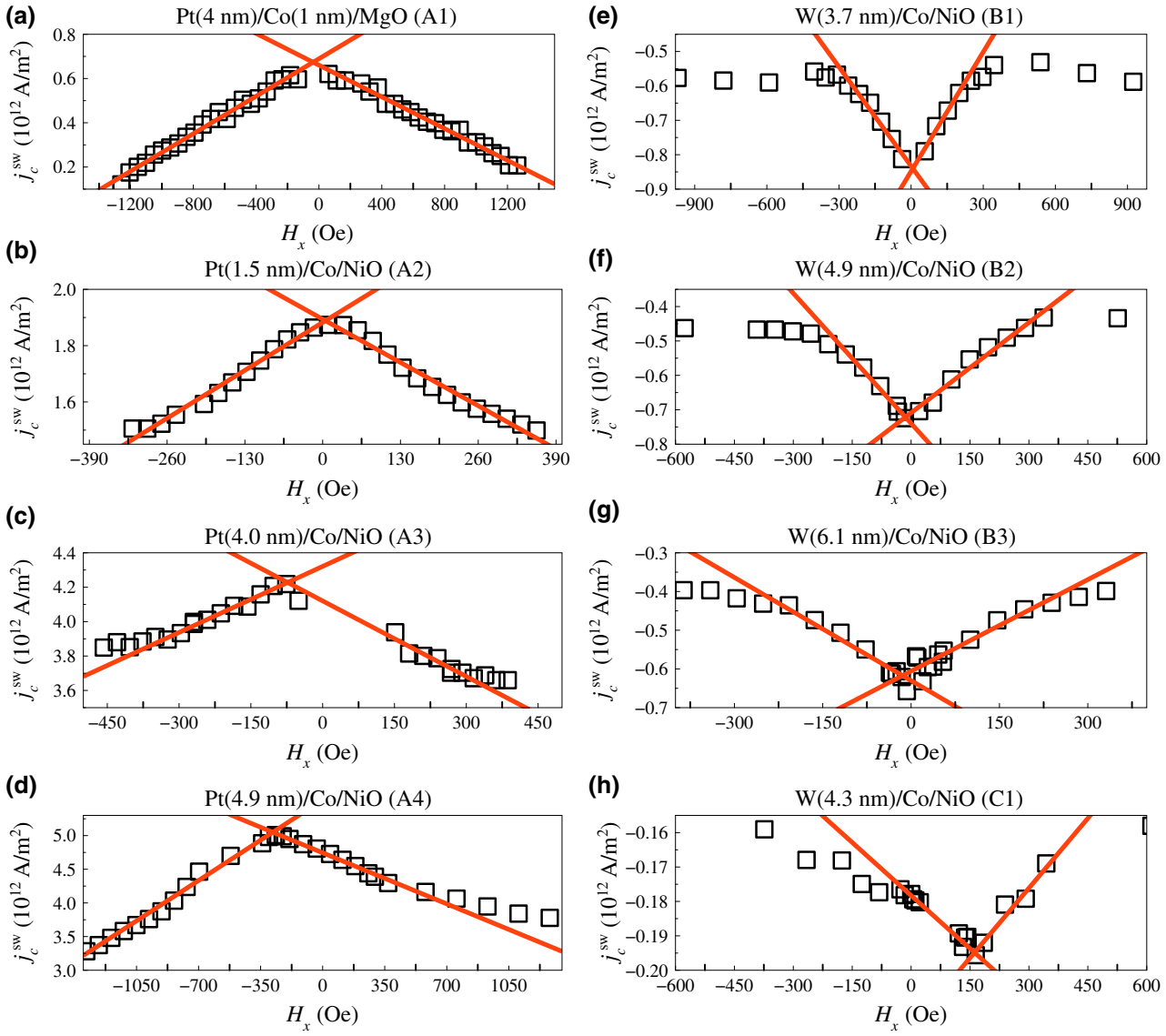

FIG. 6. Critical switching-current densities, j_c^{sw}, as a function of applied external magnetic field H_x for Pt/Co/NiO (a)–(d) and W/Co/NiO (e)–(h) differing by the HM layer thickness. (h) The annealed W-based system. The red line represents the model equation fitted to the data points. Parameters used for theoretical-model lines are given in Table I.

leads to degradation of the $H_{exb}^{(x)}$ component. The same $H_{exb}^{(x)}$-reduction effect on switching without an external magnetic field was noticed by Razavi *et al.* [29]. Then, by applying an in-plane H_x field of -200 Oe, we repeated the multiple switching events. It turns out that as the number of switching cycles increases, $H_{exb}^{(x)}$ rises to 430 Oe after 25 switching loops as depicted in Fig. 8(c). Finally, the AHE loop shapes and $H_{exb}^{(z)}$ in both systems are analyzed by our comparing the loops before and after the current-switching experiments. No significant degradation of PMA is found; however, $H_{exb}^{(z)}$ is reduced in both cases, as shown in Fig. 9, to 0 and -3 Oe, respectively for Pt-based and W-based devices. We conclude that during the switching events, significant Joule heating is generated, which may lead to the temperature increase above T_N. If an in-plane magnetic field is applied, an increase of in-plane exchange bias is accompanied by a decrease of the perpendicular exchange-bias component.

V. SUMMARY

In summary, the SOT-induced magnetization switching of W (Pt)/Co/NiO with a perpendicularly magnetized Co layer and various HM thicknesses is examined. Both the in-plane $H_{exb}^{(x)}$ and the perpendicular $H_{exb}^{(z)}$ exchange bias are determined by current-driven-switching, magnetoresistance, and AHE methods. We demonstrate in the

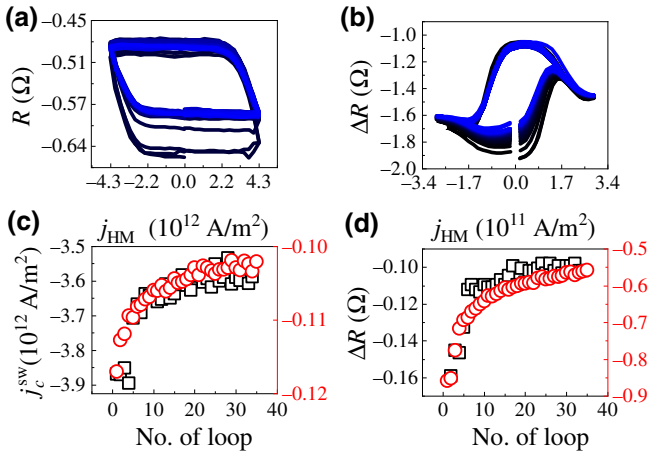

FIG. 7. A series of successive switching loops in a measurement sequence for Pt(5.1 nm)/Co(0.7 nm)/NiO(7 nm) (a) and the annealed W(4.3 nm)/Co(0.7 nm)/NiO(7 nm) device (b). The color of each subsequent loop in the sequence changes with increasing magnetic field from black to blue. Critical switching current, j_c^{sw}, versus number of repeated loops (c) and magnetoresistance, ΔR, (d) for Pt-based devices (black points) and W-based devices (red points).

Pt/Co/NiO and W/Co/NiO systems deterministic Co magnetization switching without an external magnetic field, which is replaced by an in-plane exchange-bias field. For several selected Hall-bar devices in both systems, threshold current densities are analyzed on the basis of our theoretical model, allowing us to estimate effective parameters $\theta_{SH,eff}$ and $H_{K,eff}$. Because of higher $\theta_{SH,eff}$ in the W-based system than in the Pt-based system, a critical

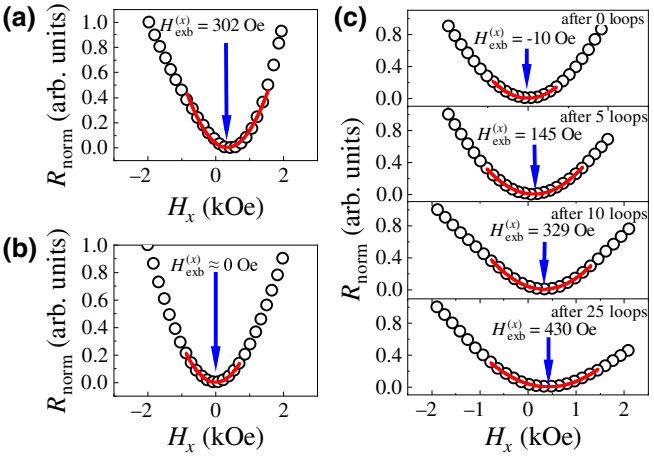

FIG. 8. Normalized longitudinal magnetoresistance of the Pt(5.1 nm)/Co(0.7 nm)/NiO(7 nm) device: (a) before the current-switching experiment, (b) after current switching without an external magnetic field, and (c) measured after a specified number of switching cycles. The red line corresponds to a quadratic function fitted to the data to determine the shift.

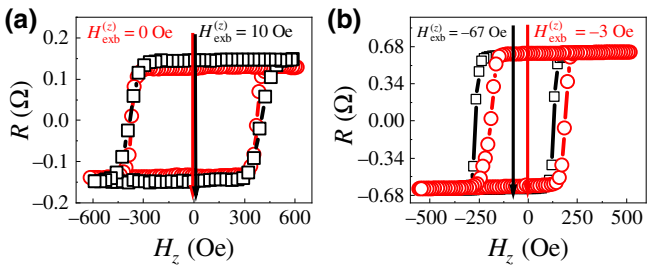

FIG. 9. AHE loops before switching experiments (black points) and after multiple switching cycles (red points) for Pt(5.1 nm)/Co(0.7 nm)/NiO(7 nm) (a) and the annealed W(4.3 nm)/Co(0.7 nm)/NiO(7 nm) (b) system.

switching-current density approximately 1 order of magnitude smaller is found. The switching stability experiments confirm the ability to induce $H_{exb}^{(x)}$ by thermal effects. Finally, we show a wide range of resistance changes in field-free magnetization switching in the case of the W (Pt)/Co/NiO system.

ACKNOWLEDGMENTS

This work was supported by the National Science Centre, Poland, Grant No. 2016/23/B/ST3/01430 (SPINORBITRONICS). W.S. acknowledges National Science Centre Grant No. 2015/17/D/ST3/00500. J.K. and W.P. acknowledge National Science Centre Grant No. 2012/05/E/ST7/00240. P.K. and M.K. acknowledge National Science Centre Grant No. 2015/18/E/ST3/00557. The authors express their gratitude to Dr. A. Kozioł-Rachwał and Dr. M. Ślęzak for fruitful discussions and technical assistance with the XAS measurements. Nanofabrication was performed at the Academic Center for Materials and Nanotechnology of AGH University of Science and Technology. The XAS experiment was performed at the SOLARIS National Synchrotron Radiation Centre Grant No. XAS–192051.

[1] A. Brataas and K. M. D. Hals, Spin–orbit torques in action, Nat. Nanotechnol. **9**, 86 (2014).
[2] T. Wang, J. Q. Xiao, and X. Fan, Spin–orbit torques in metallic magnetic multilayers: Challenges and new opportunities, SPIN **07**, 1740013 (2017).
[3] B. Dieny *et al.*, Opportunities and challenges for spintronics in the microelectronics industry, Nat. Electron. **3**, 446 (2020).
[4] K. Garello, C. O. Avci, I. M. Miron, M. Baumgartner, A. Ghosh, S. Auffret, O. Boulle, G. Gaudin, and P. Gambardella, Ultrafast magnetization switching by spin-orbit torques, Appl. Phys. Lett. **105**, 212402 (2014).
[5] S. Fukami, T. Anekawa, C. Zhang, and H. Ohno, A spin–orbit torque switching scheme with collinear magnetic

easy axis and current configuration, Nat. Nanotechnol. **11**, 621 (2016).

[6] E. Grimaldi, V. Krizakova, G. Sala, F. Yasin, S. Couet, G. Sankar Kar, K. Garello, and P. Gambardella, Single-shot dynamics of spin–orbit torque and spin transfer torque switching in three-terminal magnetic tunnel junctions, Nat. Nanotechnol. **15**, 111 (2020).

[7] J. E. Hirsch, Spin Hall Effect, Phys. Rev. Lett. **83**, 1834 (1999).

[8] S. Zhang, Spin Hall Effect in the Presence of Spin Diffusion, Phys. Rev. Lett. **85**, 393 (2000).

[9] J. Sinova, S. O. Valenzuela, J. Wunderlich, C. H. Back, and T. Jungwirth, Spin hall effects, Rev. Mod. Phys. **87**, 1213 (2015).

[10] Y. Fan, P. Upadhyaya, X. Kou, M. Lang, S. Takei, Z. Wang, J. Tang, L. He, L.-T. Chang, M. Montazeri, G. Yu, W. Jiang, T. Nie, R. N. Schwartz, Y. Tserkovnyak, and K. L. Wang, Magnetization switching through giant spin–orbit torque in a magnetically doped topological insulator heterostructure, Nat. Mater. **13**, 699 (2014).

[11] A. Manchon, J. Železný, I. Miron, T. Jungwirth, J. Sinova, A. Thiaville, K. Garello, and P. Gambardella, Current-induced spin-orbit torques in ferromagnetic and antiferromagnetic systems, Rev. Mod. Phys. **91**, 035004 (2019).

[12] K. Cai, M. Yang, H. Ju, S. Wang, Y. Ji, B. Li, K. W. Edmonds, Y. Sheng, B. Zhang, N. Zhang, S. Liu, H. Zheng, and K. Wang, Electric field control of deterministic current-induced magnetization switching in a hybrid ferromagnetic/ferroelectric structure, Nat. Mater. **16**, 712 (2017).

[13] Y.-C. Lau, D. Betto, K. Rode, J. M. D. Coey, and P. Stamenov, Spin–orbit torque switching without an external field using interlayer exchange coupling, Nat. Nanotechnol. **11**, 758 (2016).

[14] S. Łazarski, W. Skowroński, J. Kanak, Ł. Karwacki, S. Zietek, K. Grochot, T. Stobiecki, and F. Stobiecki, Field-Free Spin-Orbit-Torque Switching in Co/Pt/Co Multilayer with Mixed Magnetic Anisotropies, Phys. Rev. Appl. **12**, 014006 (2019).

[15] S.-h. C. Baek, V. P. Amin, Y.-W. Oh, G. Go, S.-J. Lee, G.-H. Lee, K.-J. Kim, M. D. Stiles, B.-G. Park, and K.-J. Lee, Spin currents and spin–orbit torques in ferromagnetic trilayers, Nat. Mater. **17**, 509 (2018).

[16] Y. Sheng, K. W. Edmonds, X. Ma, H. Zheng, and K. Wang, Adjustable current-induced magnetization switching utilizing interlayer exchange coupling, Adv. Electron. Mater. **4**, 1800224 (2018).

[17] X. Wang, C. Wan, W. Kong, X. Zhang, Y. Xing, C. Fang, B. Tao, W. Yang, L. Huang, H. Wu, M. Irfan, and X. Han, Field-free programmable spin logics via chirality-reversible spin–orbit torque switching, Adv. Mater. **30**, 1801318 (2018).

[18] T. Chuang, C. Pai, and S. Huang, Cr -induced Perpendicular Magnetic Anisotropy and Field-Free Spin-Orbit-Torque Switching, Phys. Rev. Appl. **11**, 061005 (2019).

[19] Y. Cao, A. Rushforth, Y. Sheng, H. Zheng, and K. Wang, Tuning a binary ferromagnet into a multistate synapse with spin–orbit-Torque-Induced plasticity, Adv. Funct. Mater. **29**, 1808104 (2019).

[20] S. Chen, J. Yu, Q. Xie, X. Zhang, W. Lin, L. Liu, J. Zhou, X. Shu, R. Guo, Z. Zhang, and J. Chen, Free field electric switching of perpendicularly magnetized thin film by spin current gradient, ACS Appl. Mater. Interfaces **11**, 30446 (2019).

[21] C. K. Safeer, E. Jué, A. Lopez, L. Buda-Prejbeanu, S. Auffret, S. Pizzini, O. Boulle, I. M. Miron, and G. Gaudin, Spin–orbit torque magnetization switching controlled by geometry, Nat. Nanotechnol. **11**, 143 (2016).

[22] L. You, O. Lee, D. Bhowmik, D. Labanowski, J. Hong, J. Bokor, and S. Salahuddin, Switching of perpendicularly polarized nanomagnets with spin orbit torque without an external magnetic field by engineering a tilted anisotropy, Proc. Natl. Acad. Sci. **112**, 10310 (2015).

[23] G. Yu, L.-T. Chang, M. Akyol, P. Upadhyaya, C. He, X. Li, K. L. Wong, P. K. Amiri, and K. L. Wang, Current-driven perpendicular magnetization switching in Ta/CoFeB/[TaOx or MgO/TaOx] films with lateral structural asymmetry, Appl. Phys. Lett. **105**, 102411 (2014).

[24] G. Yu, P. Upadhyaya, Y. Fan, J. G. Alzate, W. Jiang, K. L. Wong, S. Takei, S. A. Bender, L.-T. Chang, Y. Jiang, M. Lang, J. Tang, Y. Wang, Y. Tserkovnyak, P. K. Amiri, and K. L. Wang, Switching of perpendicular magnetization by spin–orbit torques in the absence of external magnetic fields, Nat. Nanotechnol. **9**, 548 (2014).

[25] S. Maat, K. Takano, S. S. P. Parkin, and E. E. Fullerton, Perpendicular Exchange Bias of Co/Pt Multilayers, Phys. Rev. Lett. **87**, 087202 (2001).

[26] Y.-W. Oh, S.-h. Chris Baek, Y. M. Kim, H. Y. Lee, K.-D. Lee, C.-G. Yang, E.-S. Park, K.-S. Lee, K.-W. Kim, G. Go, J.-R. Jeong, B.-C. Min, H.-W. Lee, K.-J. Lee, and B.-G. Park, Field-free switching of perpendicular magnetization through spin–orbit torque in antiferromagnet/ferromagnet/oxide structures, Nat. Nanotechnol. **11**, 878 (2016).

[27] S. Fukami, C. Zhang, S. DuttaGupta, A. Kurenkov, and H. Ohno, Magnetization switching by spin–orbit torque in an antiferromagnet–ferromagnet bilayer system, Nat. Mater. **15**, 535 (2016).

[28] A. van den Brink, G. Vermijs, A. Solignac, J. Koo, J. Kohlhepp, H. Swagten, and B. Koopmans, Field-free magnetization reversal by spin-hall effect and exchange bias, Nat. Commun. **7**, 10854 (2016).

[29] S. A. Razavi, D. Wu, G. Yu, Y.-C. Lau, K. L. Wong, W. Zhu, C. He, Z. Zhang, J. M. D. Coey, P. Stamenov, P. Khalili Amiri, and K. L. Wang, Joule Heating Effect on Field-Free Magnetization Switching by Spin-Orbit Torque in Exchange-Biased Systems, Phys. Rev. Appl. **7**, 024023 (2017).

[30] A. Manchon, Spin diffusion and torques in disordered antiferromagnets, J. Phys.: Condens. Matter **29**, 104002 (2017).

[31] P. Kuświk, M. Matczak, M. Kowacz, K. Szuba-Jabński, N. Michalak, B. Szymański, A. Ehresmann, and F. Stobiecki, Asymmetric domain wall propagation caused by interfacial dzyaloshinskii-moriya interaction in exchange biased Au/Co/NiO layered system, Phys. Rev. B **97**, 024404 (2018).

[32] P. Kuświk, A. Gaul, M. Urbaniak, M. Schmidt, J. Aleksiejew, A. Ehresmann, and F. Stobiecki, Tailoring perpendicular exchange bias coupling in Au/Co/NiO systems by ion bombardment, Nanomaterials **8**, 813 (2018).

[33] P. Mazalski, B. Anastaziak, P. Kuświk, Z. Kurant, I. Sveklo, and A. Maziewski, Demagnetization of an ultrathin Co/NiO bilayer with creation of submicrometer domains controlled by temperature-induced changes of magnetic anisotropy, J. Magn. Magn. Mater. **508**, 166871 (2020).

[34] P. Kuświk, B. Szymański, B. Anastaziak, M. Matczak, M. Urbaniak, A. Ehresmann, and F. Stobiecki, Enhancement of perpendicular magnetic anisotropy of Co layer in exchange-biased Au/Co/NiO/Au polycrystalline system, J. Appl. Phys. **119**, 215307 (2016).

[35] H. Yang, S.-H. Yang, D.-C. Qi, A. Rusydi, H. Kawai, M. Saeys, T. Leo, D. J. Smith, and S. S. P. Parkin, Negative Tunneling Magnetoresistance by Canted Magnetization in MgO / NiO Tunnel Barriers, Phys. Rev. Lett. **106**, 167201 (2011).

[36] K. Ono, H. Shimada, S.-i. Kobayashi, and Y. Ootuka, Magnetoresistance of Ni/NiO/Co small tunnel junctions in coulomb blockade regime, J. Phys. Soc. Jpn. **65**, 3449 (1996).

[37] A. Sokolov, I. F. Sabirianov, E. Y. Tsymbal, B. Doudin, X. Z. Li, and J. Redepenning, Resonant tunneling in magnetoresistive Ni/NiO/Co nanowire junctions, J. Appl. Phys. **93**, 7029 (2003).

[38] T. Moriyama, S. Takei, M. Nagata, Y. Yoshimura, N. Matsuzaki, T. Terashima, Y. Tserkovnyak, and T. Ono, Antidamping spin transfer torque through epitaxial nickel oxide, Appl. Phys. Lett. **106**, 162406 (2015).

[39] J. Wu, J. S. Park, W. Kim, E. Arenholz, M. Liberati, A. Scholl, Y. Z. Wu, C. Hwang, and Z. Q. Qiu, Direct Measurement of Rotatable and Frozen CoO Spins in Exchange Bias System of CoO/Fe/Ag (001), Phys. Rev. Lett. **104**, 217204 (2010).

[40] M. Ślęzak, T. Ślęzak, P. Dróżdż, B. Matlak, K. Matlak, A. Kozioł-Rachwał, M. Zając, and J. Korecki, How a ferromagnet drives an antiferromagnet in exchange biased CoO/Fe(110) bilayers, Sci. Rep. **9**, 889 (2019).

[41] See Supplemental Material at http://link.aps.org/supplemental/10.1103/PhysRevApplied.15.014017 for a detailed description of the structural characterization, the resistivity analysis, x-ray-absorption-spectroscopy measurements, the spin Hall angle, and perpendicular-exchange-bias analysis.

[42] A. Tan, J. Li, C. A. Jenkins, E. Arenholz, A. Scholl, C. Hwang, and Z. Q. Qiu, Exchange bias in epitaxially grown CoO/MgO/Fe/Ag(001), Phys. Rev. B **86**, 064406 (2012).

[43] A. Kozioł-Rachwał, W. Janus, M. Szpytma, P. Dróżdż, M. Ślęzak, K. Matlak, M. Gajewska, T. Ślęzak, and J. Korecki, Interface engineering towards enhanced exchange interaction between Fe and FeO in Fe/MgO/FeO epitaxial heterostructures, Appl. Phys. Lett. **115**, 141603 (2019).

[44] J. Zhu, Q. Li, J. X. Li, Z. Ding, J. H. Liang, X. Xiao, Y. M. Luo, C. Y. Hua, H.-J. Lin, T. W. Pi, Z. Hu, C. Won, and Y. Z. Wu, Antiferromagnetic spin reorientation transition in epitaxial NiO/CoO/MgO(001) systems, Phys. Rev. B **90**, 054403 (2014).

[45] Q. Li, J. H. Liang, Y. M. Luo, Z. Ding, T. Gu, Z. Hu, C. Y. Hua, H.-J. Lin, T. W. Pi, S. P. Kang, C. Won, and Y. Z. Wu, Antiferromagnetic proximity effect in epitaxial CoO/NiO/MgO(001) systems, Sci. Rep. **6**, 22355 (2016).

[46] F. Smits, Measurement of sheet resistivities with the four-point probe, Bell Syst. Tech. J. **34**, 711 (1958).

[47] M. Kawaguchi, D. Towa, Y.-C. Lau, S. Takahashi, and M. Hayashi, Anomalous spin hall magnetoresistance in Pt/Co bilayers, Appl. Phys. Lett. **112**, 202405 (2018).

[48] E. Sagasta, Y. Omori, M. Isasa, M. Gradhand, L. E. Hueso, Y. Niimi, Y. Otani, and F. Casanova, Tuning the spin hall effect of Pt from the moderately dirty to the superclean regime, Phys. Rev. B **94**, 060412 (2016).

[49] W. Skowroński, Ł. Karwacki, S. Zietek, J. Kanak, S. Łazarski, K. Grochot, T. Stobiecki, P. Kuświk, F. Stobiecki, and J. Barnaś, Determination of Spin Hall Angle in Heavy-Metal/Co-Fe-B-based Heterostructures with Interfacial Spin-Orbit Fields, Phys. Rev. Appl. **11**, 024039 (2019).

[50] Q. Hao, W. Chen, and G. Xiao, Beta (β) tungsten thin films: Structure, electron transport, and giant spin hall effect, Appl. Phys. Lett. **106**, 182403 (2015).

[51] Q. Hao and G. Xiao, Giant Spin Hall Effect and Switching Induced by Spin-Transfer Torque in a $W/Co_{40}Fe_{40}B_{20}/MgO$ Structure with Perpendicular Magnetic Anisotropy, Phys. Rev. Appl. **3**, 034009 (2015).

[52] L. Neumann, D. Meier, J. Schmalhorst, K. Rott, G. Reiss, and M. Meinert, Temperature dependence of the spin hall angle and switching current in the nc − W(O)/CoFeB/MgO system with perpendicular magnetic anisotropy, Appl. Phys. Lett. **109**, 142405 (2016).

[53] K.-S. Lee, S.-W. Lee, B.-C. Min, and K.-J. Lee, Threshold current for switching of a perpendicular magnetic layer induced by spin hall effect, Appl. Phys. Lett. **102**, 112410 (2013).

[54] T. Taniguchi, Theoretical condition for switching the magnetization in a perpendicularly magnetized ferromagnet via the spin hall effect, Phys. Rev. B **100**, 174419 (2019).

[55] M. Baumgartner, K. Garello, J. Mendil, C. O. Avci, E. Grimaldi, C. Murer, J. Feng, M. Gabureac, C. Stamm, Y. Acremann, S. Finizio, S. Wintz, J. Raabe, and P. Gambardella, Spatially and time-resolved magnetization dynamics driven by spin–orbit torques, Nat. Nanotechnol. **12**, 980 (2017).

[56] J. Kim, P. Sheng, S. Takahashi, S. Mitani, and M. Hayashi, Spin Hall Magnetoresistance in Metallic Bilayers, Phys. Rev. Lett. **116**, 097201 (2016).

[57] J.-C. Rojas-Sánchez, N. Reyren, P. Laczkowski, W. Savero, J.-P. Attané, C. Deranlot, M. Jamet, J.-M. George, L. Vila, and H. Jaffrès, Spin Pumping and Inverse Spin Hall Effect in Platinum: The Essential Role of Spin-Memory Loss at Metallic Interfaces, Phys. Rev. Lett. **112**, 106602 (2014).

[58] C. F. Pai, L. Liu, Y. Li, H. W. Tseng, D. C. Ralph, and R. A. Buhrman, Spin transfer torque devices utilizing the giant spin hall effect of tungsten, Appl. Phys. Lett. **101**, 122404 (2012).

[59] Y. Takeuchi, C. Zhang, A. Okada, H. Sato, S. Fukami, and H. Ohno, Spin-orbit torques in high-resistivity-W/CoFeB/MgO, Appl. Phys. Lett. **112**, 192408 (2018).

[60] S. Cho, S.-h. C. Baek, K.-D. Lee, Y. Jo, and B.-G. Park, Large spin hall magnetoresistance and its correlation to the spin-orbit torque in W/CoFeB/MgO structures, Sci. Rep. **5**, 14668 (2015).

[61] C. Zhang, S. Fukami, K. Watanabe, A. Ohkawara, S. DuttaGupta, H. Sato, F. Matsukura, and H. Ohno, Critical role of w deposition condition on spin-orbit torque induced magnetization switching in nanoscale W/CoFeB/MgO, Appl. Phys. Lett. **109**, 192405 (2016).

[62] W. Skowroński, M. Cecot, J. Kanak, S. Ziętek, T. Stobiecki, L. Yao, S. van Dijken, T. Nozaki, K. Yakushiji, and S. Yuasa, Temperature dependence of spin-orbit torques in W/CoFeB bilayers, Appl. Phys. Lett. **109**, 062407 (2016).

[63] W. Chen, G. Xiao, Q. Zhang, and X. Zhang, Temperature study of the giant spin hall effect in the bulk limit of β-W, Phys. Rev. B **98**, 134411 (2018).

[64] R. Bansal, G. Nirala, A. Kumar, S. Chaudhary, and P. K. Muduli, Large spin hall angle in β-W thin films grown on CoFeB without oxygen plasma, SPIN **8**, 1850018 (2018).

[65] O. L. W. McHugh, W. F. Goh, M. Gradhand, and D. A. Stewart, Impact of impurities on the spin hall conductivity in β -W, Phys. Rev. Mater. **4**, 094404 (2020).

[66] K. Zhang, T. Zhao, and H. Fujiwara, Training effect of exchange biased iron–oxide/ferromagnet systems, J. Appl. Phys. **89**, 6910 (2001).

[67] S. Brems, K. Temst, and C. Van Haesendonck, Origin of the Training Effect and Asymmetry of the Magnetization in Polycrystalline Exchange Bias Systems, Phys. Rev. Lett. **99**, 067201 (2007).

[68] C. Binek, Training of the exchange-bias effect: A simple analytic approach, Phys. Rev. B **70**, 014421 (2004).

[69] A. Hochstrat, C. Binek, and W. Kleemann, Training of the exchange-bias effect in nio-fe heterostructures, Phys. Rev. B **66**, 092409 (2002).